



# An immune-stimulating proteoglycan from the medicinal mushroom Huaier up-regulates NF- $\kappa$ B and MAPK signaling via Toll-like receptor 4

Received for publication, August 22, 2018, and in revised form, December 31, 2018. Published, Papers in Press, January 2, 2019, DOI 10.1074/jbc.RA118.005477

Ailin Yang<sup>†1</sup>, Haitao Fan<sup>§1</sup>, Yanan Zhao<sup>‡</sup>, Xiaonan Chen<sup>‡</sup>, Zhixiang Zhu<sup>‡</sup>, Xiaojun Zha<sup>¶</sup>, Yunfang Zhao<sup>‡</sup>, Xingyun Chai<sup>‡</sup>, Jun Li<sup>‡</sup>, Pengfei Tu<sup>‡2</sup>, and Zhongdong Hu<sup>‡3</sup>

From the <sup>‡</sup>Modern Research Center for Traditional Chinese Medicine, School of Chinese Materia Medica, Beijing University of Chinese Medicine, No. 11 North Third Ring Road, Chaoyang District, Beijing 100029, China, the <sup>§</sup>College of Bioengineering, Beijing Polytechnic, Beijing 100029, China, and the <sup>¶</sup>Department of Biochemistry and Molecular Biology, School of Basic Medicine, Anhui Medical University, Hefei 230032, China

Edited by Xiao-Fan Wang

*Trametes robiniophila* Murr. (Huaier) is a mushroom with a long history of use as a medicinal ingredient in China and exhibits good clinical efficacy in cancer management. However, the antitumor components of Huaier and the underlying molecular mechanisms remain poorly understood. Here, we isolated a proteoglycan with a molecular mass of  $\sim 5.59 \times 10^4$  Da from Huaier aqueous extract. We named this proteoglycan TPG-1, and using FTIR and additional biochemical analyses, we determined that its total carbohydrate and protein compositions are 43.9 and 41.2%, respectively. Using biochemical assays and immunoblotting, we found that exposing murine RAW264.7 macrophages to TPG-1 promotes the production of nitric oxide (NO), tumor necrosis factor  $\alpha$  (TNF $\alpha$ ), and interleukin-6 (IL-6) through Toll-like receptor 4 (TLR4)-dependent activation of NF- $\kappa$ B and mitogen-activated protein kinase (MAPK) signaling. Of note, the TPG-1 treatment significantly inhibited the tumorigenesis of human hepatoma HepG2 cells likely at least in part by increasing serum levels of TNF $\alpha$  and promoting leukocyte infiltration into tumors in nude mice. TPG-1 also exhibited good antitumor activity in hepatoma H22-bearing mice and had no obvious adverse effects in these mice. We conclude that TPG-1 exerts antitumor activity partially through an immune-potentiating effect due to activation of the TLR4–NF- $\kappa$ B/MAPK signaling cassette. Therefore, TPG-1 may be a promising candidate drug for cancer immunotherapy. This study has identified the TPG-1 proteoglycan as an antitumor agent and provided insights into TPG-1's molecular mechanism, suggesting a potential utility for applying this agent in cancer therapy.

*Trametes robiniophila* Murr. (Huaier) is a medicinal fungus that has been applied for disease treatment for more than 1600 years in China. Numerous studies have shown that Huaier

exhibits good clinical efficacy in the treatment of liver cancer, gastric cancer, prostate cancer, colon cancer, breast cancer, and lung cancer (1–4). There is evidence that some polysaccharides of Huaier aqueous extract show anti-tumor and immunomodulatory activities. For example, the crude polysaccharides of Huaier retarded the proliferation and invasive potential of human hepatocellular carcinoma MHCC97-H cells via the AEG-1/EMT pathway (5). Huaier polysaccharide TP-1 restrained the growth and metastasis of hepatocellular carcinoma at least partially through inactivating HIF-1 $\alpha$ /vascular endothelial growth factor and AUF-1/AEG-1 signaling pathways (6). In addition, Huaier polysaccharide W-NTRP suppressed the cell viability of human cholangiocarcinoma cells and promoted the proliferation of mouse splenocytes (7). However, the anti-neoplastic components in Huaier and underlying molecular mechanisms remain poorly understood.

Enhancement of immunity plays a vital role in cancer therapy in response to anti-tumor drugs. Recently, it has garnered increasing attention that polysaccharides/proteoglycans from natural sources inhibit tumor growth through activating immunologic effector cells, such as macrophages, and it is a promising strategy for the exploitation of anti-tumor drugs from polysaccharides/proteoglycans with immunopotentiating effect (8–11).

In this study, the proteoglycan TPG-1 with a molecular mass of  $\sim 5.59 \times 10^4$  Da was isolated from Huaier aqueous extract. We demonstrated that the supernatants from murine macrophage-like RAW264.7 cells treated with TPG-1 showed dramatic cytotoxicity to human hepatoma HepG2 and SK-HEP-1 cells. Moreover, TPG-1 promoted the secretion of NO,<sup>4</sup> tumor

This work was supported by National Natural Science Foundation of China Grant 81403147 and Fundamental Research Funds for the Central Universities Grant 2015-JYB-XYQ-004. The authors declare that they have no conflicts of interest with the contents of this article.

<sup>1</sup> Both authors contributed equally to this work.

<sup>2</sup> To whom correspondence may be addressed. Tel./Fax: 86-10-82802750; E-mail: pengfeitu@163.com.

<sup>3</sup> To whom correspondence may be addressed. Tel./Fax: 86-10-64286180; E-mail: zdhu@bucm.edu.cn.

<sup>4</sup> The abbreviations used are: NO, nitric oxide; FBS, fetal bovine serum; TLR4, Toll-like receptor 4; MAPK, mitogen-activated protein kinase; TNF- $\alpha$ , tumor necrosis factor- $\alpha$ ; IL-6, interleukin-6; qRT-PCR, quantitative real-time PCR; IHC, immunohistochemistry; iNOS, inducible nitric-oxide synthase; COX-2, cyclooxygenase-2; ELSD, evaporative light scattering detection; GPC, gel permeation chromatography; AFM, atomic force microscopy; ERK, extracellular signal-regulated kinase; JNK, c-Jun N-terminal kinase; p-, phosphorylated; iNOS, inducible nitric-oxide synthase; H&E, hematoxylin and eosin; ROS, reactive oxygen species; DMEM, Dulbecco's modified Eagle's medium; 5-FU, 5-fluorouracil; MTT, 3-(4,5-dimethylthiazol-2-yl)-2,5-diphenyltetrazolium bromide; Xyl, xylose; Ara, arabinose; Rha, rhamnose; Man, mannose; PNGase F, peptide:N-glycosidase F; i.p., intraperitoneally.

necrosis factor  $\alpha$  (TNF $\alpha$ ), and interleukin-6 (IL-6) through TLR4-dependent activation of NF- $\kappa$ B and MAPK signaling pathways in murine macrophage-like RAW264.7 cells. Furthermore, TPG-1 treatment significantly blunted the tumorigenic ability of HepG2 or H22 cells likely partially through facilitating the infiltration of leukocytes into tumors in mice.

## Results

### Isolation, purification, and characterization of the proteoglycan TPG-1

The saccharide fraction (TS) was obtained from Huaier aqueous extract by water extraction, deproteinization, and ethanol precipitation. The saccharide fraction was further eluted successively on a DEAE-cellulose (DE-52) column with water and 1.0 M NaCl solution, leading to the isolation of pre-TPG-1. Pre-TPG-1 eluted by water was further purified on a Sepharose CL-6B column, suggesting only one main fraction named as TPG-1. Then it was collected and freeze-dried for further studies.

The chromatogram detected by HPLC-GPC showed a single symmetrical peak (Fig. 1A), suggesting that TPG-1 was homogeneous. The average molecular mass of TPG-1 was calculated to be  $\sim 5.59 \times 10^4$  Da. The total carbohydrate content of TPG-1 was 43.93%, as measured by the phenol-sulfoacid method.

The FTIR spectrum of TPG-1 displayed a strong and broad absorption peak around  $3408 \text{ cm}^{-1}$ , which is a characteristic of N–H stretching vibrations of protein and hydroxyl groups of the polysaccharide. Weak absorption frequencies characterized around  $2921 \text{ cm}^{-1}$  and  $2851 \text{ cm}^{-1}$  were implied as bending vibrations and C–H stretching vibrations. The intense absorption peaks at  $1651.61$ ,  $1401.08$ , and  $1261.74 \text{ cm}^{-1}$  containing C–O stretching vibrations and N–H bending vibrations of acylamino were assigned to amides I, II, and III, respectively. The specific band at  $1043 \text{ cm}^{-1}$  was due to O–H variable-angle vibration of the pyranose ring (Fig. 1B).

TPG-1 was treated with 0.1 M NaOH for inducing  $\beta$ -elimination, which selectively releases O-linked saccharides connected to threonine and/or serine residues. After release of the O-glycans by NaOH, the serine and threonine were turned into aminoacrylic acid and amino crotonic acid, which enhance the absorbance at 240 nm. The results indicated that there was no presence of O-linked glycan in TPG-1 (Fig. 1C).

The molecular mass of TPG-1 treated with PNGase F detected by MALDI-TOF-MS was decreased, indicating that TPG-1 contained N-glycosidic linkage. It further implied that TPG-1 was a glycoprotein (Fig. 1, D and E).

Methylation analysis was used to illuminate the specific interglycosidic linkages between the monosaccharide residues of TPG-1. The individual peaks of TPG-1 from the GC-MS analysis were identified by their retention time and by comparison with the mass spectrum. As summarized in Table 1, TPG-1 contained glucose (Glc), xylose (Xyl), arabinose (Ara), rhamnose (Rha), galactose (Gal), and mannose (Man). Our results showed the presence of six linked types, namely 2,4,6-Me<sub>3</sub>-Glc, 2,3,4-Me<sub>3</sub>-Xyl, 2,3,4-Me<sub>3</sub>-Ara, 2,4-Me<sub>2</sub>-Rha, 4-Me-Gal, and 4,6-Me<sub>2</sub>-Man, in a molar ratio of 19.40:24.55:17.86:1.04:8.81:7.22.

In addition, amino acid analysis showed that the total amino acid content of TPG-1 was 41.20%. There were 17 kinds of amino acids in TPG-1, and the major amino acid was glutamic acid (7.42%), followed by aspartic acid, glycine, arginine, threonine, alanine, proline, and serine. Moreover, the total essential amino acid content of TPG-1 was 9.93%. TPG-1 contained six kinds of essential amino acids, such as lysine, phenylalanine, threonine, isoleucine, leucine, and valine (Table 2). The secondary structure of TPG-1 was determined by CD spectrum, and the results indicated that TPG-1 displayed a random coil conformation in aqueous solution (Fig. 1F).

Microstructure observation of TPG-1 was performed by atomic force microscopy (AFM). The results demonstrated that TPG-1 aggregated to form random chain structures to rodlike lumps, which were uniformly dispersed in aqueous solution, with diameter ranging from 200 to 800 nm and height ranging from 0.8 to 3.3 nm (Fig. 1G).

### Effects of TPG-1 on the proliferation of human hepatoma HepG2 and SK-HEP-1 cells in vitro

We first cultured human hepatoma HepG2 cells with the supernatants from RAW264.7 cells treated with or without TPG-1 or with fresh complete medium with or without TPG-1 at different time points. As shown in Fig. 2A, TPG-1 weakly inhibited the proliferation of HepG2 cells, compared with the control group. However, the supernatants from RAW264.7 cells treated with TPG-1 showed dramatic cytotoxicity in HepG2 cells in a time-dependent manner, compared with the supernatants from RAW264.7 cells untreated with TPG-1. In addition, the consistent result was obtained in human hepatoma SK-HEP-1 cells (Fig. 2B). We speculated that the phenomenon might be due to secreted factors from RAW264.7 cells induced by TPG-1.

### Effects of TPG-1 on the NO production in RAW264.7 cells

NO is one of the most versatile players in immune responses (12). We examined the effect of TPG-1 on NO production by RAW264.7 cells. We found that TPG-1 showed no cytotoxicity to RAW264.7 cells up to a concentration of 250  $\mu\text{g/ml}$  for 24 h. However, TPG-1 weakly inhibited the proliferation of RAW 264.7 cells with the extension of treatment time (Fig. 3A). The NO production by RAW264.7 cells was significantly stimulated by TPG-1 treatment not in a dose-dependent manner (Fig. 3B). Compared with the control group ( $4.85 \pm 0.34 \mu\text{M}$ ), the NO concentrations in supernatants from RAW264.7 cells were dramatically increased to  $22.63 \pm 0.45$ ,  $23.09 \pm 0.49$ ,  $23.54 \pm 0.52$ , and  $23.93 \pm 1.18 \mu\text{M}$  by treatment with TPG-1 at the concentrations of 50, 100, 250, and 500  $\mu\text{g/ml}$ , respectively. Mechanistically, our work revealed that TPG-1 up-regulated mRNA and protein levels of inducible nitric-oxide synthase (iNOS) in RAW264.7 cells (Fig. 3, C and D).

### TPG-1 increased the expression of TNF $\alpha$ , IL-6, and COX-2 in RAW264.7 cells

To further investigate the immunological activity of TPG-1, we examined the expression and secretion of TNF $\alpha$  and IL-6 in RAW264.7 cells exposed to TPG-1 by quantitative real-time PCR (qRT-PCR) and ELISA. TPG-1 treatment significantly up-regulated the mRNA levels of TNF $\alpha$  in RAW264.7 cells (Fig.

# Cancer immunotherapy of TPG-1 via TLR4–NF- $\kappa$ B/MAPK signaling

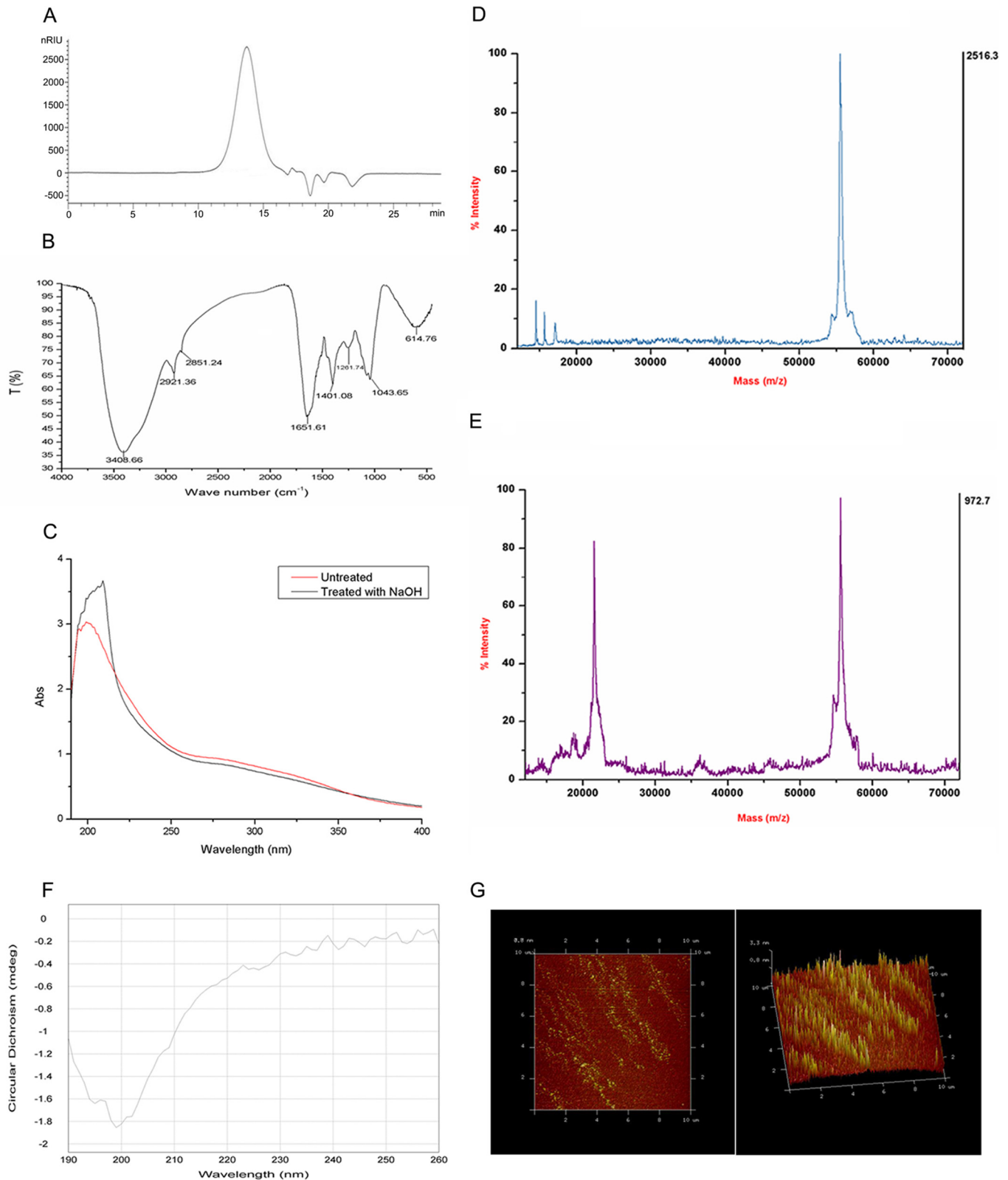


**Figure 1. Characterization of the proteoglycan TPG-1.** *A*, high-performance gel-permeation chromatography of the proteoglycan TPG-1 from Huaier. *B*, FTIR spectrum of TPG-1. *C*, UV spectrum of TPG-1. *D* and *E*, analysis of TPG-1 by MALDI-TOF-MS. *F*, CD spectrum of TPG-1. *G*, microstructure observation of TPG-1.

4A), and TNF $\alpha$  secretion was also increased in a dose-dependent manner after treatment with TPG-1 in RAW264.7 cells (Fig. 4B). Moreover, TPG-1 dramatically enhanced the expression and secretion of IL-6 in RAW264.7 cells (Fig. 4, C and D).

Cyclooxygenase-2 (COX-2) is one of the immune factors released by activated macrophages (13, 14). As depicted in Fig. 4 (E and F), TPG-1 treatment led to an increase in the mRNA and protein levels of COX-2 in RAW264.7 cells.

**Table 1**  
Methylation analysis of TPG-1

Methylation sugar	Retention time	Molar ratio	Mass fragments ( <i>m/z</i> )	Linkage type
	<i>min</i>			
2,4,6-Me <sub>3</sub> -Glc	34.98	19.40	43, 57, 71, 85, 101, 117, 128, 161	1 → 3
2,3,4-Me <sub>3</sub> -Xyl	37.81	24.55	43, 57, 71, 88, 101, 115, 128, 141, 159, 173	1 → 6
2,3,4-Me <sub>3</sub> -Ara	39.55	17.86	43, 71, 88, 101, 115, 127, 145, 187, 218	1 → 6
2,4-Me <sub>2</sub> -Rha	40.15	1.04	43, 75, 117, 131, 189	1 → 3
4-Me-Gal	47.95	8.81	43, 74, 87, 101, 111, 129, 143, 154, 173, 187, 201	1 → 2,3,6
4,6-Me <sub>2</sub> -Man	51.16	7.22	43, 57, 87, 101, 117, 128, 145, 161, 184, 205	1 → 2,3

**Table 2**  
Amino acid composition of TPG-1

Amino acid	Amino acid composition
	%
Asp	5.41
Thr	2.51
Ser	2.25
Glu	7.42
Gly	4.79
Ala	2.49
Cys	1.13
Val	1.80
Met	0.35
Ile	0.86
Leu	1.48
Tyr	0.80
Phe	1.06
Lys	2.23
His	1.44
Arg	2.87
Pro	2.32

### TPG-1 treatment led to TLR4-dependent activation of NF-κB and MAPK signaling pathways in RAW264.7 cells

To explore underlying mechanisms of immunological activity of TPG-1, total RNA was extracted from RAW264.7 cells treated with or without TPG-1 for RNA-Seq. As depicted in Fig. 5A, the analysis of RNA-Seq data showed the top 30 pathways modulated by TPG-1, including the Toll-like receptor signaling pathway, TNF signaling pathway, and NF-κB signaling pathway. These signaling pathways have been identified to be implicated in the regulation of immune responses (15–19). Next, we performed immunoblot analysis to confirm the effect of TPG-1 on the NF-κB signaling pathway in RAW264.7 cells. We demonstrated that TPG-1 up-regulated the phosphorylation of IKKα/β, IKBα, and p65 in RAW264.7 cells and also increased IKKβ expression (Fig. 5B), indicating that TPG-1 activated the NF-κB signaling pathway. Additionally, the MAPK signaling pathway is frequently reported to be involved in activation of macrophages (20–22). TPG-1 treatment markedly augmented the phosphorylation of p38, ERK, and JNK in RAW264.7 cells (Fig. 5C). Therefore, the results suggested that TPG-1-induced immune enhancement was through activation of NF-κB and MAPK signaling pathways in RAW264.7 cells.

RNA-Seq results indicated that the Toll-like receptor signaling pathway is one of the main pathways regulated by TPG-1. Moreover, there is much evidence that Toll-like receptor 4 (TLR4) is essential for activation of NF-κB and MAPK signaling (10, 22–24). Thus, next we investigated whether TLR4 was implicated in TPG-1-induced activation of NF-κB and MAPK signaling pathways. As shown in Fig. 5D, the increased expression of p-IKKα/β, IKKβ, p-p65, iNOS, and COX-2 induced by TPG-1 was noticeably inhibited by treatment with TAK-242, a

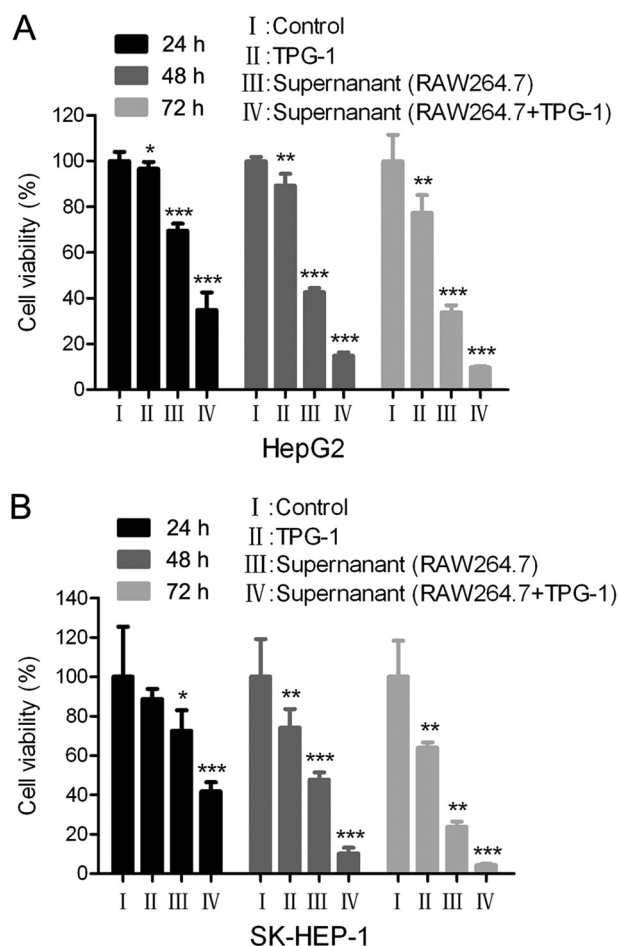


**Figure 2. Cytotoxicity of the supernatants from TPG-1-treated RAW264.7 cells to human hepatoma HepG2 and SK-HEP-1 cells.** HepG2 (A) or SK-HEP-1 (B) cells were cultured with the supernatants from RAW264.7 cells treated with or without 100 μg/ml TPG-1 for 24 h or fresh complete medium with or without 100 μg/ml TPG-1 for 24, 48, or 72 h, respectively. Cell viability was measured by the MTT assay. The data are representative of three independent experiments, and each was performed at least in triplicate. \*,  $p < 0.05$ ; \*\*,  $p < 0.01$ ; \*\*\*,  $p < 0.001$ . Error bars, confidence interval.

TLR4 inhibitor (25), in RAW264.7 cells. In addition, up-regulated MAPK signaling in RAW264.7 cells exposed to TPG-1 was remarkably impaired by TAK-242 treatment (Fig. 5E). Therefore, activation of NF-κB and MAPK induced by TPG-1 was TLR4-dependent in RAW264.7 cells.

### Up-regulation of TNFα, IL-6, and NO induced by TPG-1 were mediated by TLR4

We next investigated whether TLR4 was implicated in up-regulation of TNFα, IL-6, and NO induced by TPG-1 in RAW264.7 cells. The increased secretion of TNFα induced by

## Cancer immunotherapy of TPG-1 via TLR4–NF- $\kappa$ B/MAPK signaling

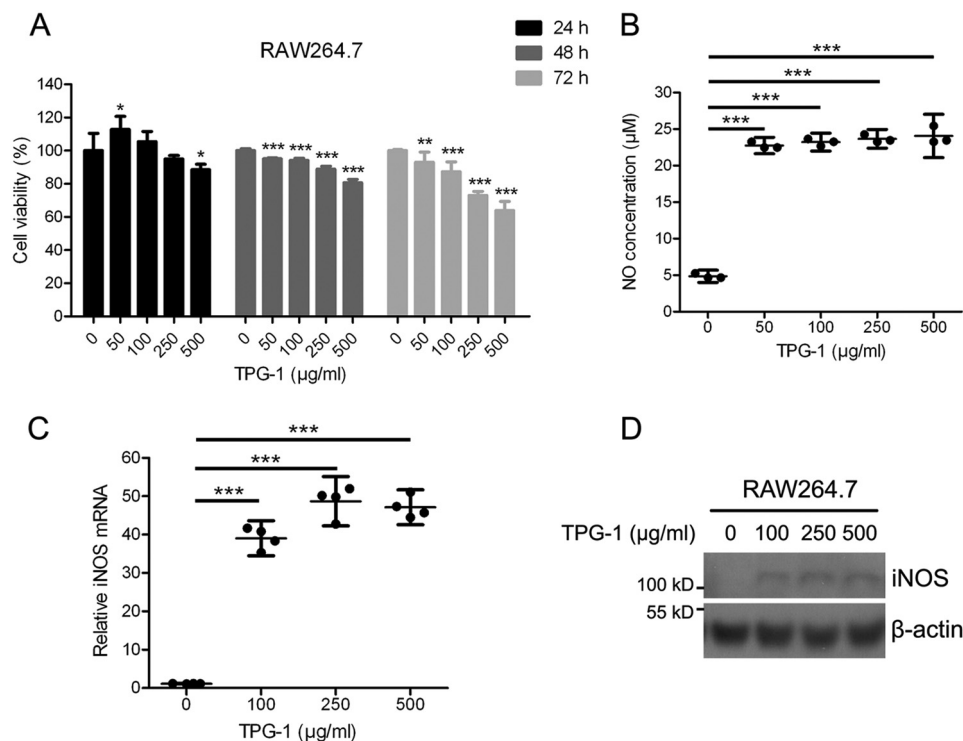


**Figure 3. Effects of TPG-1 on the NO production and iNOS activity in RAW264.7 cells.** A, RAW264.7 cells were treated with 0–500 µg/ml TPG-1 (0, 50, 100, 250, 500 µg/ml TPG-1) for 24, 48, and 72 h, respectively. Cell viability was measured by the MTT assay. B, the level of NO produced by RAW264.7 cells treated with 0–500 µg/ml TPG-1 for 24 h was examined through a Griess reaction. C and D, total RNA and cell lysates were extracted from RAW264.7 cells treated with 0–500 µg/ml TPG-1 for 24 h and subjected to quantitative real-time PCR (C) and immunoblotting (D), respectively. The data are representative of three independent experiments, and each was performed at least in triplicate. \*,  $p < 0.05$ ; \*\*,  $p < 0.01$ ; \*\*\*,  $p < 0.001$ . Error bars, confidence interval.

TPG-1 was significantly inhibited by treatment with TAK-242 in RAW264.7 cells (Fig. 6A). Similar results were also observed in the secretion of IL-6 or NO in RAW264.7 cells treated with TPG-1 in the absence or presence of TAK-242 (Fig. 6, B and C). Moreover, RNAi was used to explore whether TLR4 was involved in the increased levels of TNF $\alpha$ , IL-6, and NO in RAW264.7 cells exposed to TPG-1. TLR4 expression was modestly decreased in RAW264.7 cells transfected with siRNAs targeting TLR4 (Fig. 6D), and depletion of TLR4 led to no change on the proliferation of RAW264.7 cells (Fig. 6E). Consistently, the reduction of TLR4 expression attenuated the increased secretion of TNF $\alpha$ , IL-6, and NO in RAW264.7 cells exposed to TPG-1 (Fig. 6, F–H). Collectively, the increased production of TNF $\alpha$ , IL-6, and NO induced by TPG-1 treatment were mediated by TLR4 in RAW264.7 cells.

### In vivo anti-tumor activity of TPG-1

Human hepatoma HepG2 cells with high tumorigenicity were adopted to establish a xenograft tumor model used to evaluate the anti-tumor effect of TPG-1 *in vivo*. As depicted in Fig. 7A, TPG-1 treatment significantly blunted the tumorigenic capacity of HepG2 cells in nude mice. Moreover, treatment with TPG-1 led to no significant weight loss of nude mice (Fig. 7B). Additionally, H&E staining analysis suggested that TPG-1 displayed no obvious cytotoxicity on the major organs, including heart, liver, spleen, lung, and kidney (Fig. 7C). Furthermore, blood analysis revealed that there was no hematotoxicity in nude mice after treatment with TPG-1 (Fig. 7, D–F). TPG-1 treatment also increased the serum level of TNF $\alpha$  in nude mice

(Fig. 7G). As shown in Fig. 7H, immunohistochemistry (IHC) analysis for Ki67 (a proliferation marker) (26), CD45 (a leukocyte marker) (27), and F4/80 (a macrophage marker) (28) revealed that TPG-1 treatment inhibited the proliferation of HepG2 cells and facilitated the infiltration of leukocytes into tumors derived from HepG2 cells in nude mice.

We also investigated the anti-tumor effect of TPG-1 in hepatoma H22-bearing Kunming mice. As shown in Fig. 8A, TPG-1 treatment significantly inhibited the oncogenicity of mouse hepatoma H22 cells in Kunming mice. The body weight curve showed that TPG-1 treatment led to weak inhibition on the body weight of Kunming mice (Fig. 8B). Moreover, H&E staining analysis showed that TPG-1 exhibited no obvious cytotoxicity on the major organs (Fig. 8C). In addition, the IHC analysis of tumor tissues suggested that the proliferation of H22 cells in Kunming mice was suppressed by TPG-1, and TPG-1 treatment also facilitated the infiltration of leukocytes into tumors derived from H22 cells in Kunming mice (Fig. 8D). Taken together, the results supported the notion that the immunopotentiating effect of TPG-1 contributed to anti-tumor activity of TPG-1.

### Discussion

The anti-cancer effects of polysaccharides/proteoglycans from natural sources have attracted increasing attention recently. Herein, we isolated a new proteoglycan TPG-1 from Huaier aqueous extract. Further investigation revealed that TPG-1 exhibited good anti-tumor activity partially due to the

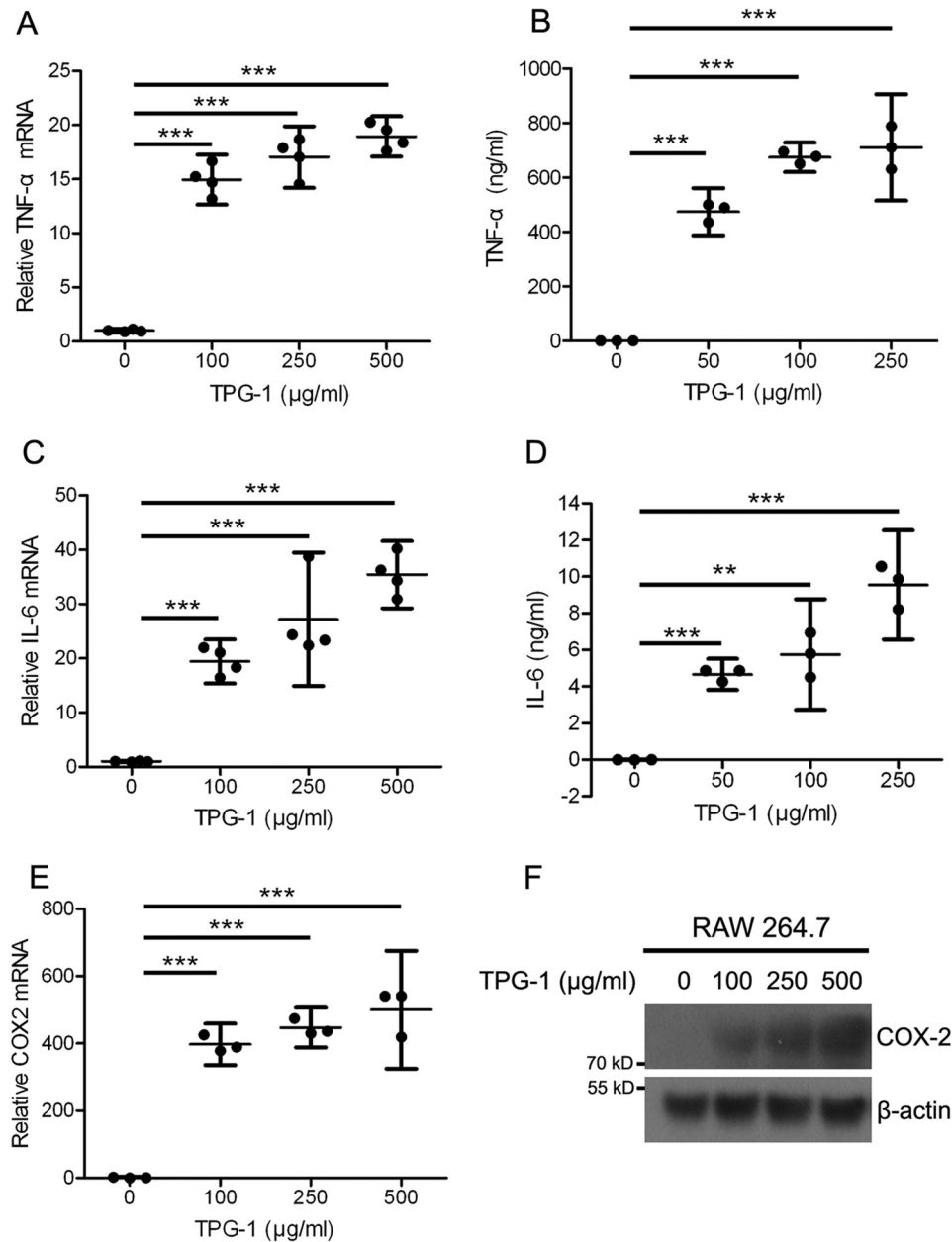


**Figure 4. Effects of TPG-1 on the expression of TNF $\alpha$ , IL-6, and COX-2 in RAW264.7 cells.** A, C, and E, total RNA were extracted from RAW264.7 cells treated with 0–500  $\mu\text{g/ml}$  TPG-1 for 24 h and subjected to quantitative real-time PCR. B and D, the levels of TNF $\alpha$  (B) or IL-6 (D) in supernatants from RAW264.7 cells treated with 0–250  $\mu\text{g/ml}$  TPG-1 for 24 h were measured by ELISA. F, cell lysates were extracted from RAW264.7 cells treated with 0–500  $\mu\text{g/ml}$  TPG-1 for 24 h and subjected to immunoblotting. The data are representative of three independent experiments, and each was performed at least in triplicate. \*\*,  $p < 0.01$ ; \*\*\*,  $p < 0.001$ . Error bars, confidence interval.

immunopotentiating effect via TLR4-dependent activation of NF-κB and MAPK signaling pathways.

Macrophages are pivotal cells of the immune system, which are crucial components for the defense against tumors by releasing some cytokines, such as NO, TNF $\alpha$ , and IL-6 (29). There is much evidence that many polysaccharides/proteoglycans enhance immune activities by promoting macrophage activation. For example, *Salicornia* polysaccharides significantly promoted NO production and iNOS transcription in RAW264.7 cells (30). A proteoglycan isolated from *Poria cocos* induced the activation of RAW 264.7 cells through up-regulation of TNF $\alpha$  (31). Additionally, it has been reported that the immunomodulatory effect is one of underlying mechanisms of

anti-tumor activity of Huaier (2, 7, 32). Our work showed that the proteoglycan TPG-1 isolated from Huaier significantly increased the production of NO, TNF $\alpha$ , and IL-6 in RAW264.7 cells. Moreover, TPG-1 treatment dramatically up-regulated the expression of iNOS and COX-2 in RAW264.7 cells. NO secretion is increased by activation of macrophages. It is an important factor for killing cancer cells in tumor immunotherapy. Moreover, activation of iNOS leads to increased production of NO in macrophages (33, 34). TNF $\alpha$  and IL-6 are both multifunctional cytokines involved in immune responses. TNF $\alpha$  produced by activated macrophages can induce tumor necrosis (35). IL-6 has been reported to be a cytokine with anti-tumor activity (36). COX-2 is a cyclooxygenase that is activated

## Cancer immunotherapy of TPG-1 via TLR4–NF-κB/MAPK signaling

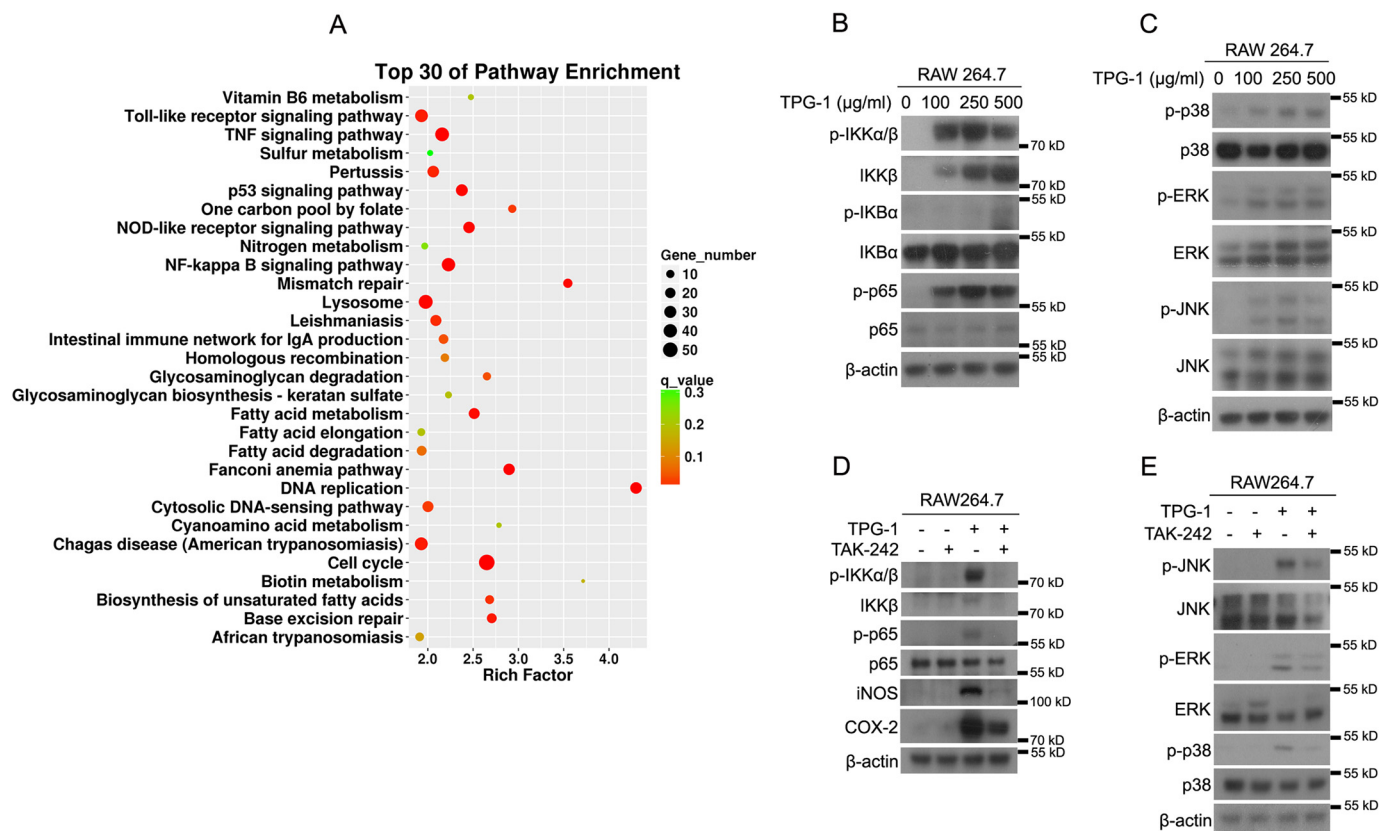


**Figure 5.** TPG-1 treatment induced TLR4-dependent activation of NF-κB and MAPK signaling in RAW264.7 cells. **A**, total RNA was extracted from RAW264.7 cells treated with or without TPG-1 and subjected to RNA sequence, and the scatter plot of differential genes from KEGG enrichment analysis is shown, including the top 30 enriched KEGG pathways. **B** and **C**, cell lysates were extracted from RAW264.7 cells treated with 0–500 μg/ml TPG-1 for 48 h and subjected to immunoblotting for the indicated proteins of the NF-κB signaling pathway or MAPK signaling pathway. **D** and **E**, cell lysates were extracted from RAW264.7 cells treated with or without 100 μg/ml TPG-1 in the absence or presence of 1 μM TAK-242 for 24 h and subjected to immunoblotting. The data are representative of three independent experiments.

in immune response. TNFα enhances COX-2 expression in macrophages, and COX-2 positively regulates the production of IL-6 (37–39). Thus, elevated COX-2 may be involved in TPG-1-induced up-regulation of IL-6. Taken together, proteoglycan TPG-1 is a potent immunostimulant.

There are many documentations on the mechanisms of enhancement of immunity by polysaccharides. *Astragalus* polysaccharides promoted the secretion of NO, TNFα, and IL-6 through activation of TLR4 signaling pathway in macrophages (10). *Sargassum fusiforme* polysaccharide induced cytokine production partially by the TLRs/NF-κB signaling pathway in macrophages (40). *Ganoderma atrum* polysaccharide (PSG-1) promoted the secretion of TNFα through up-regulation of ROS/phosphatidylinositol 3-kinase/AKT, ROS/MAPK, and ROS/NF-κB signaling pathways mediated by TLR4 (41). TLR4 plays a vital role in innate immune response and cytokine production. It has been reported that TLR4 is essential for macrophage activation in the presence of polysaccharides/proteoglycans from *Platycodon grandiflorum* and *P. cocos* (31, 42). Numerous studies demonstrated that activation of NF-κB and MAPK signaling are mediated by TLR4. Moreover, NF-κB and MAPK signaling pathways are both positive regulators of the secretion of TNFα, IL-6, and NO, as well as the expressions of iNOS and COX-2 (43–46). In this study, we demonstrated that TLR4 was required for TPG-1-induced activation of NF-κB and MAPK signaling pathways in RAW264.7 cells.

Furthermore, our work revealed that TPG-1-induced up-regulation of TNFα, IL-6, and NO were mediated by TLR4 through pharmacological and genetic approaches. Therefore, we proposed that TPG-1 exerted good immunopotentiating effect through up-regulation of a TLR4–NF-κB/MAPK signaling cassette.

The investigation of drugs for cancer immunotherapy is attracting increasing attention, such as polysaccharides/proteoglycans. Now some anti-neoplastic polysaccharide/proteoglycan drugs have been on the market or in clinical trials, such as lentinan, Krestin (PSK), and schizophyllan (8, 47, 48). We found that TPG-1 treatment significantly inhibited the tumorigenic capacity of human hepatoma HepG2 cells in a xenograft mouse model. Moreover, there were no obvious side effects on the body weight, major organs, and blood of mice after treatment with TPG-1. TNFα is closely associated with immune response and apoptosis. It has been proved that TNFα displays good clinical efficacy in cancer treatment (49, 50). Herein, we found that TPG-1 treatment increased the serum level of TNFα in nude mice, which may be responsible for the inhibition of cell proliferation in tumors derived from HepG2 cells. In addition, the supernatants from RAW264.7 cells treated with TPG-1 exhibited significant cytotoxicity to human hepatoma HepG2 and SK-HEP-1 cells. Interestingly, TPG-1 treatment observably facilitated the infiltration of leukocytes into tumors in mice. In addition, similar anti-tumor effect of

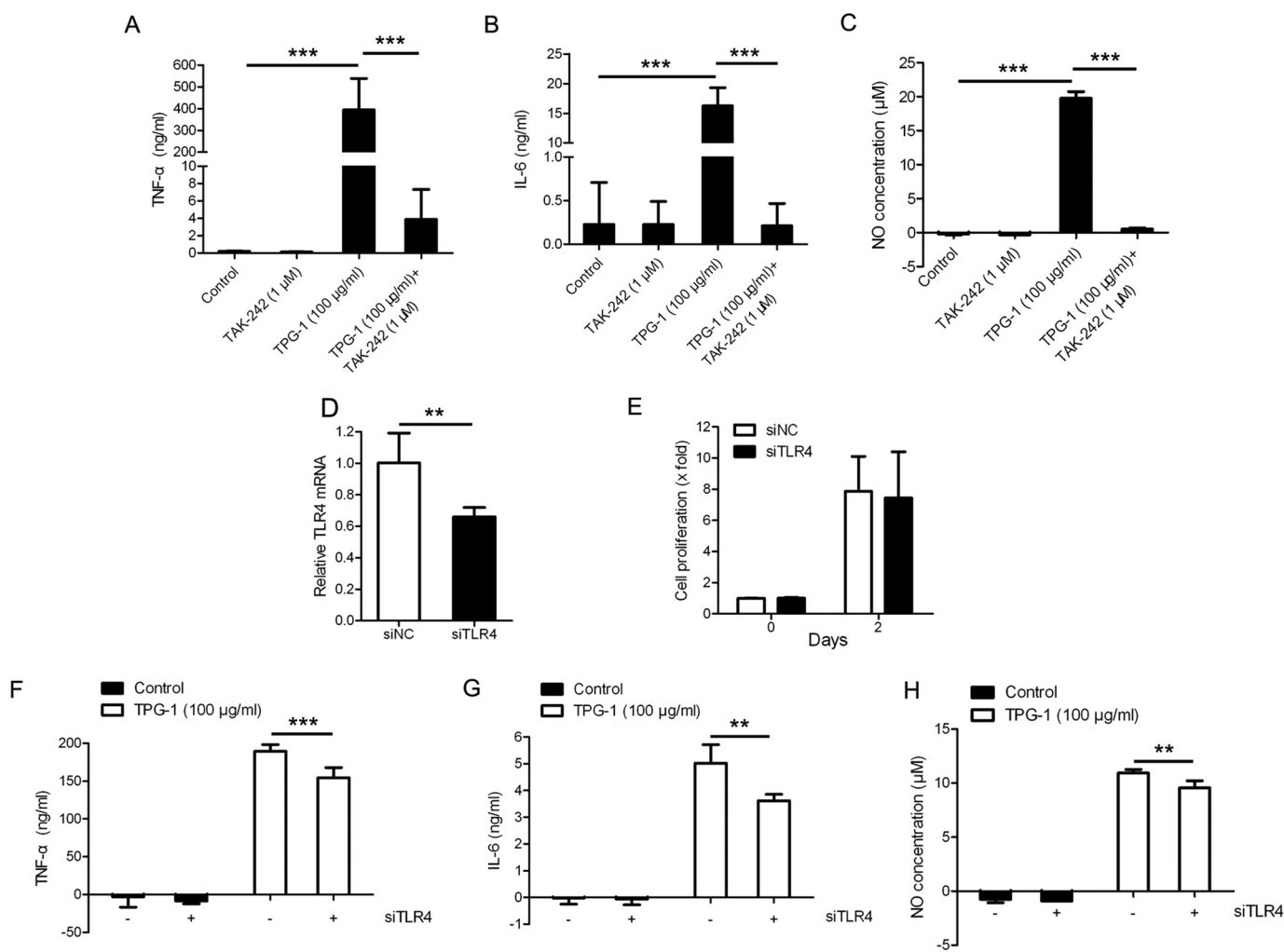


**Figure 6. Up-regulation of TNF $\alpha$ , IL-6, and NO induced by TPG-1 were mediated by TLR4.** A–C, the levels of TNF $\alpha$  (A), IL-6 (B), or NO (C) produced by RAW264.7 cells treated with or without 100  $\mu$ g/ml TPG-1 in the absence or presence of 1  $\mu$ M TAK-242 for 24 h were measured by ELISA or Griess reaction. D, total RNA were extracted from RAW264.7 cells transfected with TLR4 siRNAs or negative control siRNAs and subjected to quantitative real-time PCR. E, the proliferation of RAW264.7 cells transfected with TLR4 siRNAs or negative control siRNAs were measured by the MTT assay. F–H, RAW264.7 cells transfected with TLR4 siRNAs or negative control siRNAs were treated with or without 100  $\mu$ g/ml TPG-1 for 24 h, and the levels of TNF $\alpha$  (F), IL-6 (G), or NO (H) in the supernatants were measured by ELISA or Griess reaction. The data are representative of three independent experiments, and each was performed at least in triplicate. \*\*,  $p < 0.01$ ; \*\*\*,  $p < 0.001$ . Error bars, confidence interval.

TPG-1 was also observed in hepatoma H22-bearing Kunming mice. Collectively, TPG-1 is able to potentiate immune function *in vitro* and *in vivo*. We propose that the anti-tumor effect of TPG-1 is partially attributed to the immunoenhancement. Therefore, proteoglycan TPG-1 from Huaier may be a promising candidate drug for cancer immunotherapy.

In summary, the proteoglycan TPG-1, with a molecular mass of  $\sim 5.59 \times 10^4$  Da, was isolated from Huaier. The total carbohydrate content of TPG-1 was 43.93%, and it was composed of glucose, xylose, arabinose, rhamnose, galactose, and mannose in a molar ratio of 19.40:24.55:17.86:1.04:8.81:7.22. The protein content of TPG-1 was 41.20%, and linked to the glycan by *N*-glycosidic linkage. Moreover, we demonstrated that TPG-1 exerted good anti-tumor activity partially through the immunopotentiating effect mediated by activation of the TLR4–NF- $\kappa$ B/MAPK signaling cassette (Fig. 9). However, it is still unclear whether TPG-1 is a key ingredient toward the clinical effect of Huaier. TPG-1 may be a novel candidate drug for cancer treatment. Our work provided insights into TPG-1's molecular

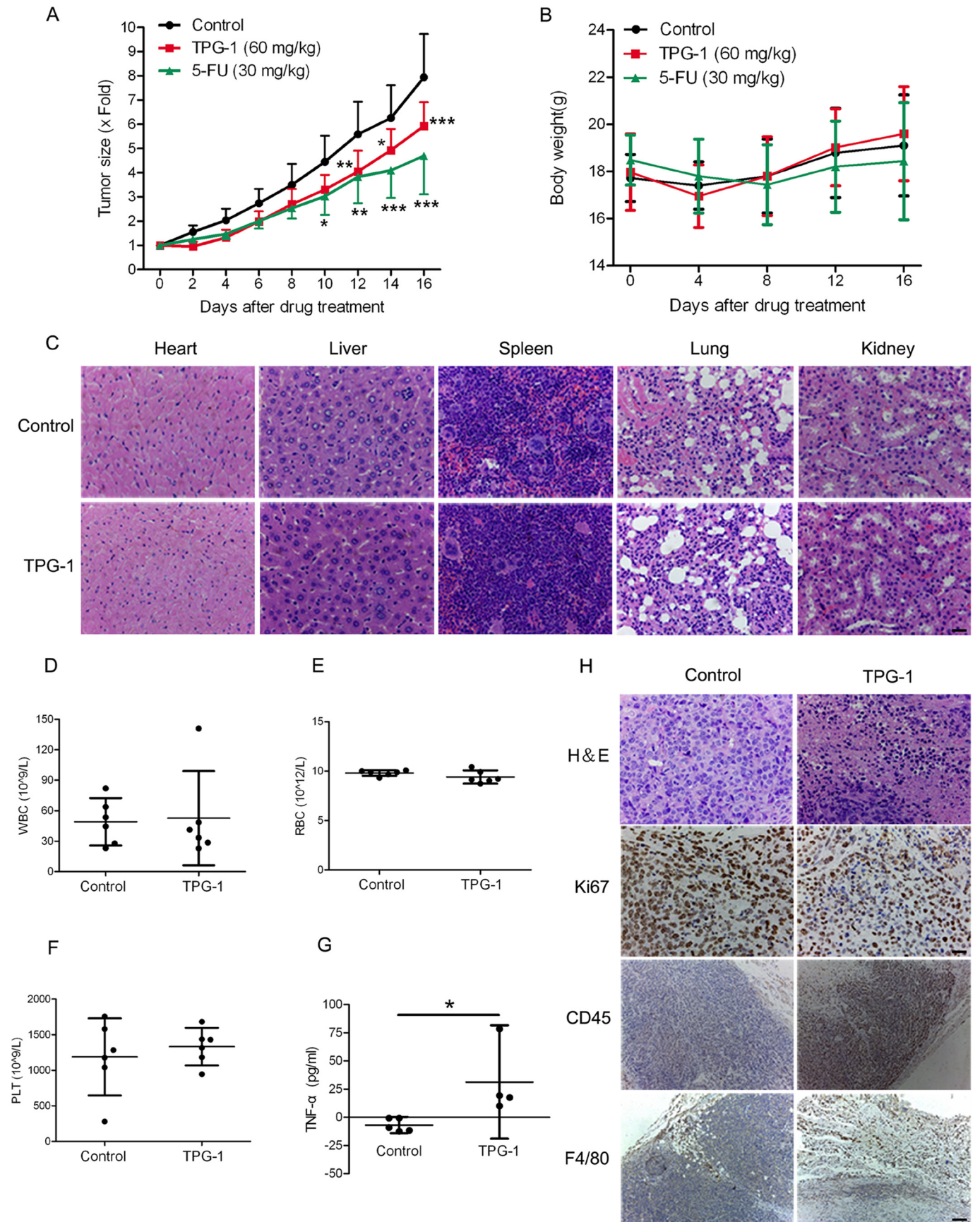
mechanism, suggesting a potential utility for applying this agent in cancer immunotherapy.

## Experimental procedures

### Reagents and antibodies

DMEM, FBS, PBS, and 0.25% trypsin-EDTA were obtained from Corning Life Sciences (Corning, NY). TAK-242 was obtained from Aladdin Shanghai Biochemical Technology Co., Ltd. (Shanghai, China). 5-FU was from Sigma (Deisenhofen, Germany). MTT was from Biodee Co., Ltd. (Beijing, China). Antibodies against iNOS (catalog no. 13120), COX-2 (catalog no. 4842), p-IKK $\alpha$ / $\beta$  (catalog no. 2697), IKK $\beta$  (catalog no. 8943), p-I $\kappa$ B $\alpha$  (catalog no. 2859), I $\kappa$ B $\alpha$  (catalog no. 4814), p-p65 (catalog no. 3033), p65 (catalog no. 8242), p-p38 (catalog no. 4511), p38 (catalog no. 8690), p-ERK1/2 (catalog no. 4370), ERK1/2 (catalog no. 4695), p-JNK (catalog no. 4668), and JNK (catalog no. 9252) were purchased from Cell Signaling Technology (Danvers, MA). Anti- $\beta$ -actin antibody (catalog no.

**Cancer immunotherapy of TPG-1 via TLR4–NF-κB/MAPK signaling**



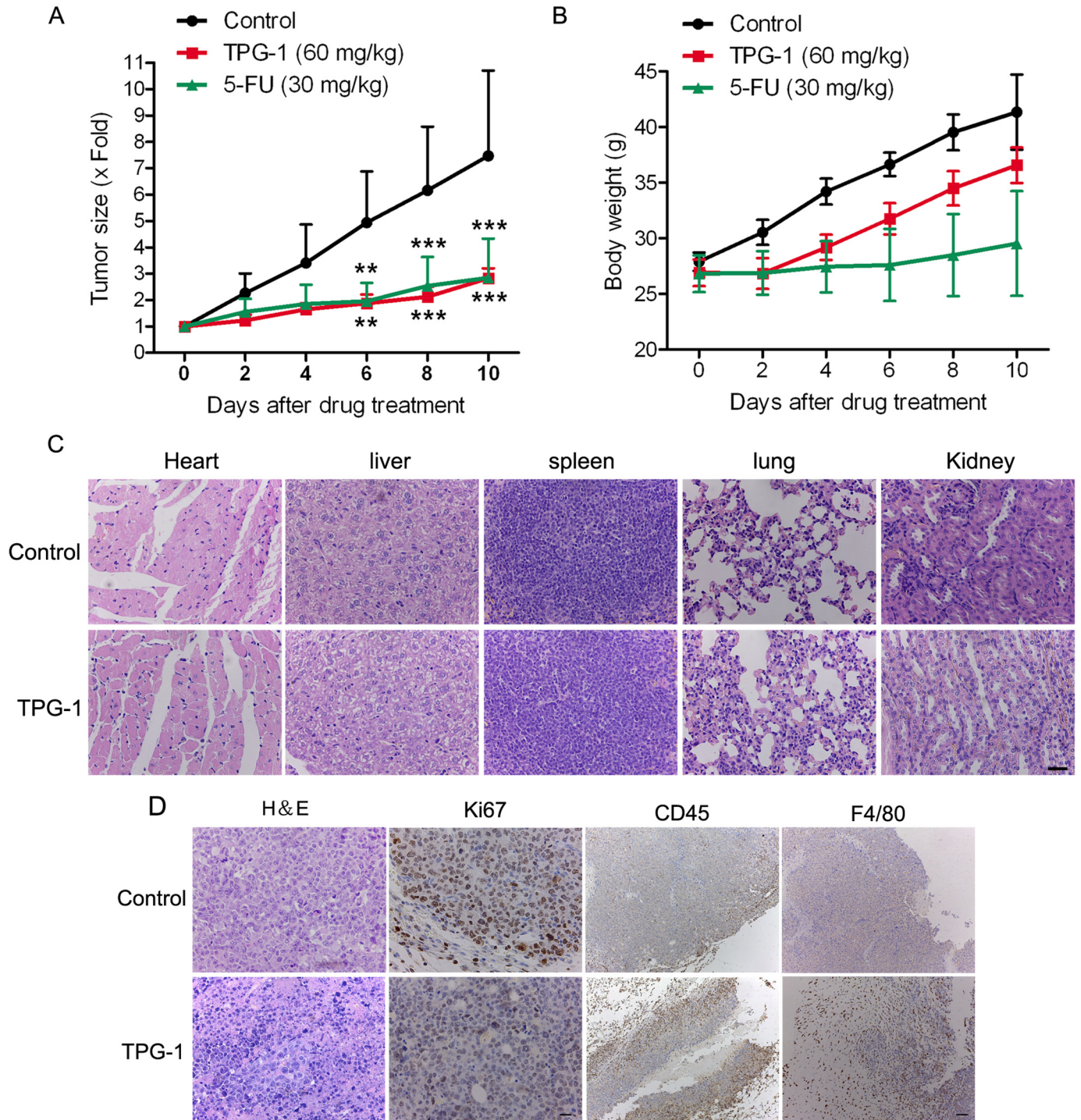


**Figure 8. TPG-1 dramatically inhibited the oncogenicity of mouse hepatoma H22 cells in Kunming mice.** *A*, hepatoma H22-bearing Kunming mice were treated with TPG-1 (i.p., 60 mg/kg, once daily) or 5-FU (i.p., 30 mg/kg, three times per week). *B*, body weight of the Kunming mice during drug treatment. *C*, H&E staining of major organs from Kunming mice treated with or without TPG-1. Scale bar, 50  $\mu$ m. *D*–*F*, number of white blood cells, red blood cells, and blood platelets from nude mice treated with or without TPG-1. *G*, serum level of TNF $\alpha$  in nude mice treated with or without TPG-1 was measured by ELISA. *H*, H&E staining and immunohistochemical analysis of tumor tissues from nude mice treated with or without TPG-1. Scale bar, 50  $\mu$ m (left) or 200  $\mu$ m (right). \*\*,  $p < 0.01$ ; \*\*\*,  $p < 0.001$ . Error bars, confidence interval.

**Figure 7. TPG-1 significantly suppressed the oncogenic capability of HepG2 cells *in vivo* without obvious side effects.** *A*, nude mice bearing HepG2 tumor xenografts were treated with TPG-1 (i.p., 60 mg/kg, once daily) or 5-FU (i.p., 30 mg/kg, three times per week). *B*, body weight of the nude mice during drug treatment. *C*, H&E staining of major organs from nude mice treated with or without TPG-1. Scale bar, 50  $\mu$ m. *D*–*F*, number of white blood cells, red blood cells, and blood platelets from nude mice treated with or without TPG-1. *G*, serum level of TNF $\alpha$  in nude mice treated with or without TPG-1 was measured by ELISA. *H*, H&E staining and immunohistochemical analysis of tumor tissues from nude mice treated with or without TPG-1. Scale bar, 50  $\mu$ m (top) or 200  $\mu$ m (bottom). \*,  $p < 0.05$ ; \*\*,  $p < 0.01$ ; \*\*\*,  $p < 0.001$ . Error bars, confidence interval.

## Cancer immunotherapy of TPG-1 via TLR4–NF- $\kappa$ B/MAPK signaling

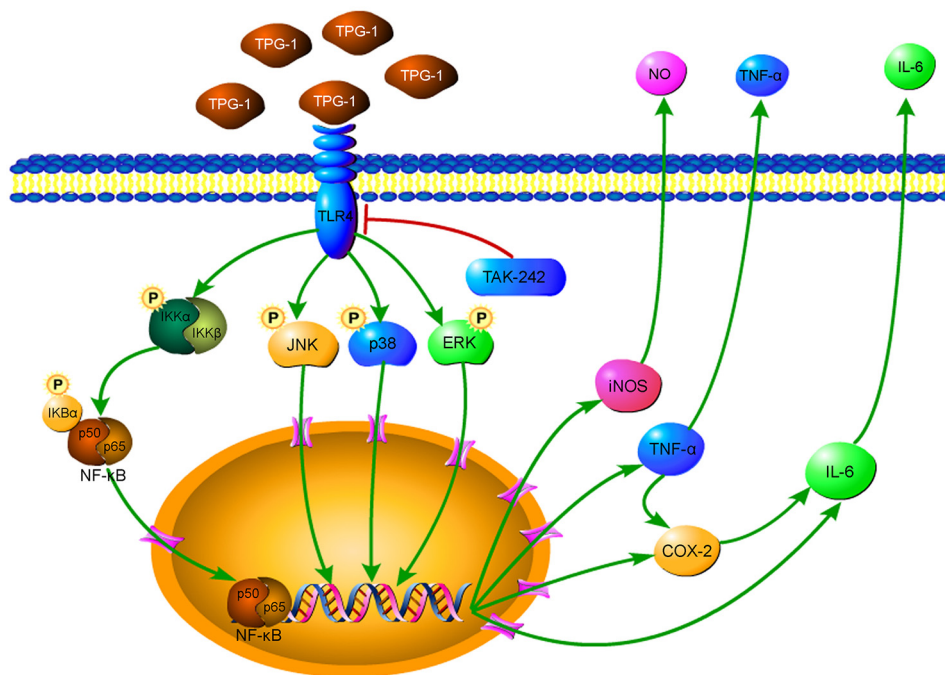


**Figure 9. Schematic illustration of the mechanisms underlying the immunopotentiating effect of the proteoglycan TPG-1 from Huaier.** TPG-1 exerted anti-tumor activity partially through the immunopotentiating effect that resulted from up-regulation of TNF $\alpha$ , IL-6, and NO, mediated by TLR4-dependent activation of NF- $\kappa$ B and MAPK signaling pathways.

sc-47778) and the horseradish peroxidase–labeled anti-mouse (catalog no. sc-2005) or rabbit (catalog no. sc-2004) antibodies were from Santa Cruz Biotechnology, Inc. (Dallas, TX).

### Cell culture

Human hepatoma cell lines SK-HEP-1 and HepG2 are from American Type Culture Collection (Manassas, VA). The murine macrophage-like cell line RAW264.7 is from the Cell Culture Center of the Institute of Basic Medical Sciences of the Chinese Academy of Medical Sciences (Beijing, China). The cells were maintained in DMEM containing 10% FBS and 1% penicillin/streptomycin at 37 °C and 5% CO<sub>2</sub>.

### Isolation and purification of the proteoglycan TPG-1

The electuary ointment of Huaier (*T. robinophila* Murr.) was obtained from Gaitianli Medicine Co., Ltd. (Jiangsu, China). The electuary ointment of Huaier was dissolved in distilled water to obtain the 8% dilute solution, and then the Sevage reagent was added to remove the free proteins (51). The precipitate separated by 60% ethanol was collected by centrifugation (3000  $\times$  *g* for 10 min) and dissolved in distilled water, and then the solution was concentrated under reduced pressure to remove excess solvent residues before vacuum freeze-drying. TS was dissolved in distilled water, and the solution was loaded onto a column of DEAE-cellulose (DE-52) and eluted successively with distilled water and 1.0 M NaCl. The fraction of 1.0 M NaCl elution was dialyzed, further separated, and purified on a Sepharose CL-6B column eluted with distilled water at a flow rate of 1 ml $\cdot$ min<sup>-1</sup> to yield one major fraction. The fraction was characterized as a single symmetrical peak by HPLC-GPC-ELSD and then freeze-dried to be a purified proteoglycan, named TPG-1.

### Characterization of the proteoglycan TPG-1

#### IR spectral analysis

The FTIR spectrum of TPG-1 was detected using the potassium bromide (KBr) disk method with an FTIR spectrometer (Jasco Corp., Tokyo, Japan) in the range of 400–4000 cm<sup>-1</sup>.

#### Glycosidic linkage analysis

TPG-1 was dissolved in 0.5 M NaBH<sub>4</sub>, 0.1 M NaOH and incubated at 25 °C for 18 h. TPG-1 without NaOH treatment was used as the control. NaOH treatment and untreated sample were detected by a UV spectrophotometer (Jasco) ranging from 200 to 400 nm. TPG-1 was dissolved in ammonium bicarbonate (NH<sub>4</sub>HCO<sub>3</sub>) (50 mM) and treated with glycosidase PNGase F (New England Biolabs) for 16 h at 37 °C. The hydrolysis reaction was terminated by heating for 10 min at 95 °C. Molecular mass was analyzed by using MALDI-TOF-MS (AB Sciex 4700). TPG-1 without glycosidase hydrolysis was used as the control.

#### Methylation analysis

The phenol-sulfoacid method was used to determine the total carbohydrate content of TPG-1. TPG-1 was completely methylated as described previously with some modifications. TPG-1 (7 mg) was dissolved in 10 ml of dried methanol and then evaporated to dryness. The dried TPG-1 was dissolved in DMSO (10 ml), mixed with NaOH (600 mg), and ultrasonicated for 2.5 h. Methyl iodide (500  $\mu$ l) was added to the reaction mixture away from light and then ultrasonicated for 10 min. The procedure was repeated three times, and the mixture was further ultrasonicated for 1 h. A total of 7 ml of distilled water and 3 ml of chloroform were added to the reaction product and then centrifuged after being shaken and mixed. The chloroform

layer was washed three times with distilled water. Subsequently, the completion of methylation was certified by the disappearance of the O–H band ( $3200\text{--}3600\text{ cm}^{-1}$ ) by FTIR. The completely methylated sample was hydrolyzed in 10 ml of 2 M TFA for 6 h. The hydrolysate was reduced with 20 mg of  $\text{NaBH}_4$  and kept at  $40\text{ }^\circ\text{C}$  for 30 min, and then the reduction action was terminated by adding to 100  $\mu\text{l}$  of glacial acetic acid. The product was acetylated with 2 ml of acetic anhydride and 2 ml of pyridine after being dried under low pressure. After incubation at  $95\text{ }^\circ\text{C}$  for 1 h, the acetylated derivatives were evaporated to dryness and extracted with 2 ml of chloroform. Finally, GC-MS (GCMS-QP 2010, Shimadzu, Kyoto, Japan) was used to analyze the alditol acetates.

### The detection of molecular weight

The average molecular mass of the proteoglycan TPG-1 was measured by HPLC-GPC-ELSD using a TSK<sup>®</sup> G5000PWXL ( $300 \times 7.8\text{ mm}$ ), eluted with deionized water at a flow rate of  $0.8\text{ ml}\cdot\text{min}^{-1}$ . The average molecular mass of the proteoglycan TPG-1 was calculated by comparison with the retention times of dextran standards (Sigma; 1, 12, 50, 80, 270, 670, and 1100 kDa).

### Amino acid composition analysis

The amino acid composition of TPG-1 was determined as follows. 15.55 mg of TPG-1 was hydrolyzed with 10 ml of 6 M HCl at  $110\text{ }^\circ\text{C}$  for 24 h. Then 1 ml of the sample was taken for drying, and 500  $\mu\text{l}$  of 0.02 M HCl was added to dissolve the sample. After centrifugation ( $12,000 \times g$  for 10 min), the supernatant was filtered, and the amino acid composition was analyzed by an L-8800 Hitachi High Speed Amino Acid Analyzer (Tokyo, Japan).

### Analysis of CD spectrum

TPG-1 was dissolved in distilled water and detected by a CD spectropolarimeter (Chirascan, Applied Photophysics, Leatherhead, UK) ranging from 190 to 260 nm at  $25\text{ }^\circ\text{C}$ .

### Microstructure observation

AFM (BioScope Catylyst NanoScope V, Bruker, Billerica, MA) was used to observe the ultrastructure of TPG-1. TPG-1 was dissolved in distilled water ( $1\text{ }\mu\text{g}/\text{ml}$ ) and stirred at room temperature for 6 h. 5  $\mu\text{l}$  of the solution was dripped to a freshly cleaved mica substrate and allowed to dry at room temperature. The AFM was determined in the contact mode. A tube-type piezoelectric scanner ( $5 \times 5\text{ }\mu\text{m}$ ) and a  $\text{Si}_3\text{N}_4$  probe (Olympus, Japan) were employed. Images were generated simultaneously with  $256 \times 256$  pixels at a scanning rate of 1.0 Hz per line.

### Cell viability assay

Cells were seeded in 96-well plates at a density of 4000–10,000 cells/well. The next day, the cells were treated with TPG-1 at the indicated concentrations for different times. Then the supernatant was removed, and MTT was added to each well at a final concentration of 0.5 mg/ml. After a 4-h incubation at  $37\text{ }^\circ\text{C}$ , 150  $\mu\text{l}$  of DMSO was added to each well, and the optical density was measured with a microplate reader (PerkinElmer Life Sciences) at 490 nm.

### RNA sequence and data analysis

Total RNA was extracted from RAW264.7 cells treated with or without TPG-1 ( $100\text{ }\mu\text{g}/\text{ml}$ ) for 24 h using TRIzol (Invitrogen) according to the manufacturer's protocol. RNA sequencing was performed on the Illumina Hiseq x Ten by Shanghai Biotechnology Corp. (Shanghai, China). Data analysis was conducted using the Hisat2 and Stringtie software.

### qRT-PCR

Total RNA was extracted from RAW264.7 cells treated with TPG-1 at the indicated concentrations for 24 h using TRIzol and then was converted into cDNA using the PrimeScript RT Reagent Kit (TaKaRa, Dalian, China) according to the manufacturer's protocol. 4  $\mu\text{l}$  of cDNA was used as a template for the quantitative PCR by using the TransStart Tip Green qPCR Kit (TransGen Biotech, Beijing, China). The primer sequences were as follows: iNOS forward, 5'-CGGCAAACATGACTTC-AGGC-3'; iNOS reverse, 5'-GCACATCAAAGCGGCCA-TAG-3'; TNF $\alpha$  forward, 5'-CCCCTTTATTGTCTACT-CCT-3'; TNF $\alpha$  reverse, 5'-AAAGCCCATTGAGTCCTTG-3'; IL-6 forward, 5'-AAATAGTCCTTCTACCCCAA-3'; IL-6 reverse, 5'-CCGAGTAGATCTCAAAGTGAC-3'; COX-2 forward, 5'-TCAATACTGGAAGCCGAGCA-3'; COX-2 reverse, 5'-CACCCCTTCACATTATTGCAGA-3'; TLR4 forward, 5'-CAAGGGATAAGAACGCTGAGA-3'; TLR4 reverse, 5'-GCAATGTCTCTGGCAGGTGTA-3'; GAPDH forward, 5'-GCGACTTCAACAGCAACTCC-3'; GAPDH reverse, 5'-CACCCCTGTTGCTGTAGCCGT-3'.

### Determination of NO

RAW264.7 cells were seeded in 96-well plates at a density of 80,000 cells/well. The next day, the cells were treated with TPG-1 at the indicated concentrations for 24 h. The amount of NO can be assessed by examining the nitrite concentration in the culture supernatants. The level of nitrite was measured through a Griess reaction with a nitric oxide assay kit (Applygen, Beijing, China) according to the manufacturer's protocol.

### ELISA

RAW264.7 cells were seeded in 6-well plates. The next day, the cells were treated with TPG-1 at the indicated concentrations for 24 h. Cell culture supernatants were collected, and the levels of TNF $\alpha$  and IL-6 secreted in the supernatants were examined with TNF $\alpha$  and IL-6 ELISA kits (Boster, Wuhan, China) according to the manufacturer's instructions.

### Immunoblotting

RAW264.7 cells were washed two times with cold PBS and harvested on ice with lysis buffer (10% glycerol, 10 mM Tris (pH 6.8), 2% SDS, and 100 mM DTT) and boiled at  $98\text{ }^\circ\text{C}$  for 10 min. The protein levels were detected by immunoblot analysis as described previously (52). In brief, cell lysates were separated by SDS-PAGE and then transferred onto polyvinylidene difluoride membranes. Subsequently, the membranes were blocked in TBST with 3–5% nonfat dry milk at room temperature for 1 h and then incubated with the primary antibodies at  $4\text{ }^\circ\text{C}$  overnight. Next, the membranes were incubated with horseradish

## Cancer immunotherapy of TPG-1 via TLR4–NF- $\kappa$ B/MAPK signaling

peroxidase-labeled secondary antibodies at room temperature for 2 h, followed by chemiluminescence detection.

### RNAi

The siRNAs were synthesized from GenePharma (Shanghai, China). RAW264.7 cells cultured in 6-well plates were transfected with siRNAs using Lipofectamine 2000 (Thermo Fisher Scientific) according to the manufacturer's protocol. The siRNA sequences were as follows: TLR4 (mouse), 5'-GAAUUGUAUCGCCUUCUUATT-3'; negative control (scrambled siRNA), 5'-UUCUCCGAACGUGUCACGUTT-3'.

### TPG-1 treatment

Nude mice (BALB/c, 4–5 weeks old) and Kunming mice (4–5 weeks old) were obtained from Beijing Vital River Laboratory Animal Technology Co., Ltd. The subcutaneous tumor model was established as described previously (53). A total of  $2 \times 10^6$  HepG2 cells or  $8 \times 10^6$  mouse hepatoma H22 cells in 200  $\mu$ l of Dulbecco's modified Eagle's medium were subcutaneously inoculated into the right posterior back region of nude mice or Kunming mice, respectively. The mice were randomized into three groups and treated with drugs by intraperitoneal injection. Six mice were used in each cohort. The three groups were as follows: (i) PBS, once daily; (ii) 60 mg/kg TPG-1, once daily; (iii) 30 mg/kg 5-FU, three times per week. Tumor growth was measured and normalized to the initial volumes. The animal experiment was performed in accordance with guidelines for the use and care of animals approved by the Beijing University of Chinese Medicine Committee of Ethics.

### Blood analysis

Blood samples were collected from nude mice treated with or without TPG-1. The number of white blood cells, red blood cells, and blood platelets were examined by the Sysmex XS-800i automated hematology analyzer (Kobe, Japan).

### IHC analysis

Immunohistochemical staining was performed as described previously (54). In brief, major organs or tumor tissues of mice treated with or without TPG-1 were fixed in 4% paraformaldehyde and then were embedded in paraffin. Subsequently, the paraffin sections were subjected to H&E staining and immunohistochemical analysis of indicated proteins.

### Statistical analysis

The two-tailed Student's *t* test was used to analyze the differences between two groups, and two-way analysis of variance was used for the comparisons of multiple groups. GraphPad Prism version 5.0 software was used for data analysis. Data represent the mean  $\pm$  95% confidence intervals in all figures. *p* < 0.05 was considered statistically significant.

**Author contributions**—A. Y. and H. F. performed the experiments, analyzed data, and wrote the manuscript. Yanan Zhao, X. Chen, Z. Z., X. Z., and Yunfang Zhao performed the experiments and analyzed data. X. Chai and J. L. analyzed data and revised the manuscript. P. T. and Z. H. conceived the project, designed experiments, and revised the manuscript. All authors have read and approved the final manuscript.

### References

1. Chen, Q., Shu, C., Laurence, A. D., Chen, Y., Peng, B. G., Zhen, Z. J., Cai, J. Q., Ding, Y. T., Li, L. Q., Zhang, Y. B., Zheng, Q. C., Xu, G. L., Li, B., Zhou, W. P., Cai, S. W., *et al.* (2018) Effect of Huaier granule on recurrence after curative resection of HCC: a multicentre, randomised clinical trial. *Gut* **67**, 2006–2016 [CrossRef Medline](#)
2. Song, X., Li, Y., Zhang, H., and Yang, Q. (2015) The anticancer effect of Huaier (Review). *Oncol. Rep.* **34**, 12–21 [CrossRef Medline](#)
3. Yang, A., Zhao, Y., Wang, Y., Zha, X., Zhao, Y., Tu, P., and Hu, Z. (2018) Huaier suppresses proliferative and metastatic potential of prostate cancer PC3 cells via downregulation of Lamin B1 and induction of autophagy. *Oncol. Rep.* **39**, 3055–3063 [Medline](#)
4. Hu, Z., Yang, A., Su, G., Zhao, Y., Wang, Y., Chai, X., and Tu, P. (2016) Huaier restrains proliferative and invasive potential of human hepatoma SKHEP-1 cells partially through decreased Lamin B1 and elevated NOV. *Sci. Rep.* **6**, 31298 [CrossRef Medline](#)
5. Zheng, J., Li, C., Wu, X., Liu, M., Sun, X., Yang, Y., Hao, M., Sheng, S., Sun, Y., Zhang, H., Long, J., Liang, Y., and Hu, C. (2014) Huaier polysaccharides suppresses hepatocarcinoma MHCC97-H cell metastasis via inactivation of EMT and AEG-1 pathway. *Int. J. Biol. Macromol.* **64**, 106–110 [CrossRef Medline](#)
6. Li, C., Wu, X., Zhang, H., Yang, G., Hao, M., Sheng, S., Sun, Y., Long, J., Hu, C., Sun, X., Li, L., and Zheng, J. (2015) A Huaier polysaccharide restrains hepatocellular carcinoma growth and metastasis by suppression angiogenesis. *Int. J. Biol. Macromol.* **75**, 115–120 [CrossRef Medline](#)
7. Sun, Y., Sun, T., Wang, F., Zhang, J., Li, C., Chen, X., Li, Q., and Sun, S. (2013) A polysaccharide from the fungi of Huaier exhibits anti-tumor potential and immunomodulatory effects. *Carbohydr. Polym.* **92**, 577–582 [CrossRef Medline](#)
8. Ooi, V. E., and Liu, F. (2000) Immunomodulation and anti-cancer activity of polysaccharide-protein complexes. *Curr. Med. Chem.* **7**, 715–729 [CrossRef Medline](#)
9. Tan, B. K., and Vanitha, J. (2004) Immunomodulatory and antimicrobial effects of some traditional chinese medicinal herbs: a review. *Curr. Med. Chem.* **11**, 1423–1430 [CrossRef Medline](#)
10. Zhou, L., Liu, Z., Wang, Z., Yu, S., Long, T., Zhou, X., and Bao, Y. (2017) Astragalus polysaccharides exerts immunomodulatory effects via TLR4-mediated MyD88-dependent signaling pathway *in vitro* and *in vivo*. *Sci. Rep.* **7**, 44822 [CrossRef Medline](#)
11. Lu, H., Yang, Y., Gad, E., Wenner, C. A., Chang, A., Larson, E. R., Dang, Y., Martzen, M., Standish, L. J., and Disis, M. L. (2011) Polysaccharide krestin is a novel TLR2 agonist that mediates inhibition of tumor growth via stimulation of CD8 T cells and NK cells. *Clin. Cancer Res.* **17**, 67–76 [CrossRef Medline](#)
12. Bogdan, C. (2001) Nitric oxide and the immune response. *Nat. Immunol.* **2**, 907–916 [CrossRef Medline](#)
13. Zhang, C. X., and Dai, Z. R. (2011) Immunomodulatory activities on macrophage of a polysaccharide from *Sipunculus nudus* L. *Food Chem. Toxicol.* **49**, 2961–2967 [CrossRef Medline](#)
14. Karnjanapratum, S., and You, S. (2011) Molecular characteristics of sulfated polysaccharides from *Monostroma nitidum* and their *in vitro* anti-cancer and immunomodulatory activities. *Int. J. Biol. Macromol.* **48**, 311–318 [CrossRef Medline](#)
15. Aderem, A., and Ulevitch, R. J. (2000) Toll-like receptors in the induction of the innate immune response. *Nature* **406**, 782–787 [CrossRef Medline](#)
16. Akira, S., and Takeda, K. (2004) Toll-like receptor signalling. *Nat. Rev. Immunol.* **4**, 499–511 [CrossRef Medline](#)
17. Akira, S., Takeda, K., and Kaisho, T. (2001) Toll-like receptors: critical proteins linking innate and acquired immunity. *Nat. Immunol.* **2**, 675–680 [CrossRef Medline](#)
18. Li, Q., and Verma, I. M. (2002) NF- $\kappa$ B regulation in the immune system. *Nat. Rev. Immunol.* **2**, 725–734 [CrossRef Medline](#)
19. Aggarwal, B. B. (2003) Signalling pathways of the TNF superfamily: a double-edged sword. *Nat. Rev. Immunol.* **3**, 745–756 [CrossRef Medline](#)
20. Mosser, D. M., and Edwards, J. P. (2008) Exploring the full spectrum of macrophage activation. *Nat. Rev. Immunol.* **8**, 958–969 [CrossRef Medline](#)

21. Long, T., Liu, Z., Shang, J., Zhou, X., Yu, S., Tian, H., and Bao, Y. (2018) *Polygonatum sibiricum* polysaccharides play anti-cancer effect through TLR4–MAPK/NF- $\kappa$ B signaling pathways. *Int. J. Biol. Macromol.* **111**, 813–821 [CrossRef Medline](#)
22. Wei, W., Xiao, H. T., Bao, W. R., Ma, D. L., Leung, C. H., Han, X. Q., Ko, C. H., Lau, C. B., Wong, C. K., Fung, K. P., Leung, P. C., Bian, Z. X., and Han, Q. B. (2016) TLR-4 may mediate signaling pathways of *Astragalus polysaccharide* RAP induced cytokine expression of RAW264.7 cells. *J. Ethnopharmacol.* **179**, 243–252 [CrossRef Medline](#)
23. Zhang, G., and Ghosh, S. (2001) Toll-like receptor-mediated NF- $\kappa$ B activation: a phylogenetically conserved paradigm in innate immunity. *J. Clin. Invest.* **107**, 13–19 [CrossRef Medline](#)
24. Pålsson-McDermott, E. M., and O'Neill, L. A. (2004) Signal transduction by the lipopolysaccharide receptor, Toll-like receptor-4. *Immunology* **113**, 153–162 [CrossRef Medline](#)
25. Matsunaga, N., Tsuchimori, N., Matsumoto, T., and Ii, M. (2011) TAK-242 (resatorvid), a small-molecule inhibitor of Toll-like receptor (TLR) 4 signaling, binds selectively to TLR4 and interferes with interactions between TLR4 and its adaptor molecules. *Mol. Pharmacol.* **79**, 34–41 [CrossRef Medline](#)
26. Guzman, G., Alagiozian-Angelova, V., Layden-Almer, J. E., Layden, T. J., Testa, G., Benedetti, E., Kajdacsy-Balla, A., and Cotler, S. J. (2005) p53, Ki-67, and serum  $\alpha$  fetoprotein as predictors of hepatocellular carcinoma recurrence in liver transplant patients. *Mod. Pathol.* **18**, 1498–1503 [CrossRef Medline](#)
27. Trowbridge, I. S., and Thomas, M. L. (1994) CD45: an emerging role as a protein tyrosine phosphatase required for lymphocyte activation and development. *Annu. Rev. Immunol.* **12**, 85–116 [CrossRef Medline](#)
28. Austyn, J. M., and Gordon, S. (1981) F4/80, a monoclonal antibody directed specifically against the mouse macrophage. *Eur. J. Immunol.* **11**, 805–815 [CrossRef Medline](#)
29. Zong, A., Cao, H., and Wang, F. (2012) Anticancer polysaccharides from natural resources: a review of recent research. *Carbohydr. Polym.* **90**, 1395–1410 [CrossRef Medline](#)
30. Lee, K. Y., Lee, M. H., Chang, I. Y., Yoon, S. P., Lim, D. Y., and Jeon, Y. J. (2006) Macrophage activation by polysaccharide fraction isolated from *Salicornia herbacea*. *J. Ethnopharmacol.* **103**, 372–378 [CrossRef Medline](#)
31. Chang, H. H., Yeh, C. H., and Sheu, F. (2009) A novel immunomodulatory protein from *Poria cocos* induces Toll-like receptor 4-dependent activation within mouse peritoneal macrophages. *J. Agric. Food Chem.* **57**, 6129–6139 [CrossRef Medline](#)
32. Li, C., Wu, X., Zhang, H., Yang, G., Hao, M., Sheng, S., Sun, Y., Long, J., Hu, C., Sun, X., Li, L., and Zheng, J. (2015) A Huaier polysaccharide inhibits hepatocellular carcinoma growth and metastasis. *Tumour Biol.* **36**, 1739–1745 [CrossRef Medline](#)
33. Aktan, F. (2004) iNOS-mediated nitric oxide production and its regulation. *Life Sci.* **75**, 639–653 [CrossRef Medline](#)
34. Wink, D. A., Hines, H. B., Cheng, R. Y., Switzer, C. H., Flores-Santana, W., Vitek, M. P., Ridnour, L. A., and Colton, C. A. (2011) Nitric oxide and redox mechanisms in the immune response. *J. Leukoc. Biol.* **89**, 873–891 [CrossRef Medline](#)
35. Locksley, R. M., Killeen, N., and Lenardo, M. J. (2001) The TNF and TNF receptor superfamilies: integrating mammalian biology. *Cell* **104**, 487–501 [CrossRef Medline](#)
36. Akira, S., Hirano, T., Taga, T., and Kishimoto, T. (1990) Biology of multifunctional cytokines: IL 6 and related molecules (IL 1 and TNF). *FASEB J.* **4**, 2860–2867 [CrossRef Medline](#)
37. Nakao, S., Ogtata, Y., Shimizu, E., Yamazaki, M., Furuyama, S., and Sugiyama, H. (2002) Tumor necrosis factor  $\alpha$  (TNF- $\alpha$ )-induced prostaglandin E2 release is mediated by the activation of cyclooxygenase-2 (COX-2) transcription via NF $\kappa$ B in human gingival fibroblasts. *Mol. Cell Biochem.* **238**, 11–18 [CrossRef Medline](#)
38. Medeiros, R., Figueiredo, C. P., Pandolfo, P., Duarte, F. S., Prediger, R. D., Passos, G. F., and Calixto, J. B. (2010) The role of TNF- $\alpha$  signaling pathway on COX-2 upregulation and cognitive decline induced by  $\beta$ -amyloid peptide. *Behav. Brain Res.* **209**, 165–173 [CrossRef Medline](#)
39. Bukata, S. V., Gelinis, J., Wei, X., Rosier, R. N., Puzas, J. E., Zhang, X., Schwarz, E. M., Song, X. Y., Griswold, D. E., and O'Keefe, R. J. (2004) PGE2 and IL-6 production by fibroblasts in response to titanium wear debris particles is mediated through a Cox-2 dependent pathway. *J. Orthop. Res.* **22**, 6–12 [CrossRef Medline](#)
40. Chen, X., Yu, G., Fan, S., Bian, M., Ma, H., Lu, J., and Jin, L. (2014) *Sargassum fusiforme* polysaccharide activates nuclear factor  $\kappa$ -B (NF- $\kappa$ B) and induces cytokine production via Toll-like receptors. *Carbohydr. Polym.* **105**, 113–120 [CrossRef Medline](#)
41. Yu, Q., Nie, S. P., Wang, J. Q., Yin, P. F., Huang, D. F., Li, W. J., and Xie, M. Y. (2014) Toll-like receptor 4-mediated ROS signaling pathway involved in *Ganoderma atrum* polysaccharide-induced tumor necrosis factor- $\alpha$  secretion during macrophage activation. *Food Chem. Toxicol.* **66**, 14–22 [CrossRef Medline](#)
42. Yoon, Y. D., Han, S. B., Kang, J. S., Lee, C. W., Park, S. K., Lee, H. S., Kang, J. S., and Kim, H. M. (2003) Toll-like receptor 4-dependent activation of macrophages by polysaccharide isolated from the radix of *Platycodon grandiflorum*. *Int. Immunopharmacol.* **3**, 1873–1882 [CrossRef Medline](#)
43. Bonizzi, G., and Karin, M. (2004) The two NF- $\kappa$ B activation pathways and their role in innate and adaptive immunity. *Trends Immunol.* **25**, 280–288 [CrossRef Medline](#)
44. Vallabhapurapu, S., and Karin, M. (2009) Regulation and function of NF- $\kappa$ B transcription factors in the immune system. *Annu. Rev. Immunol.* **27**, 693–733 [CrossRef Medline](#)
45. Pearson, G., Robinson, F., Beers Gibson, T., Xu, B. E., Karandikar, M., Berman, K., and Cobb, M. H. (2001) Mitogen-activated protein (MAP) kinase pathways: regulation and physiological functions. *Endocr. Rev.* **22**, 153–183 [CrossRef Medline](#)
46. Kawai, T., and Akira, S. (2006) TLR signaling. *Cell Death Differ.* **13**, 816–825 [CrossRef Medline](#)
47. Fisher, M., and Yang, L. X. (2002) Anticancer effects and mechanisms of polysaccharide-K (PSK): implications of cancer immunotherapy. *Anticancer Res.* **22**, 1737–1754 [Medline](#)
48. Krosli, G., and Korbelik, M. (1994) Potentiation of photodynamic therapy by immunotherapy: the effect of schizophyllan (SPG). *Cancer Lett.* **84**, 43–49 [CrossRef Medline](#)
49. Eggermont, A. M., de Wilt, J. H., and ten Hagen, T. L. (2003) Current uses of isolated limb perfusion in the clinic and a model system for new strategies. *Lancet Oncol.* **4**, 429–437 [CrossRef Medline](#)
50. Old, L. J. (1985) Tumor necrosis factor (TNF). *Science* **230**, 630–632 [CrossRef Medline](#)
51. Staub, A. M. (1965) Removal of protein-Sevag method. *Methods Carbohydr. Chem.* **5**, 5–6
52. Hu, Z., Wang, Y., Huang, F., Chen, R., Li, C., Wang, F., Goto, J., Kwiatkowski, D. J., Wdziedzick-Bakala, J., Tu, P., Liu, J., Zha, X., and Zhang, H. (2015) Brain-expressed X-linked 2 is pivotal for hyperactive mechanistic target of rapamycin (mTOR)-mediated tumorigenesis. *J. Biol. Chem.* **290**, 25756–25765 [CrossRef Medline](#)
53. Sun, Q., Chen, X., Ma, J., Peng, H., Wang, F., Zha, X., Wang, Y., Jing, Y., Yang, H., Chen, R., Chang, L., Zhang, Y., Goto, J., Onda, H., Chen, T., et al. (2011) Mammalian target of rapamycin up-regulation of pyruvate kinase isoenzyme type M2 is critical for aerobic glycolysis and tumor growth. *Proc. Natl. Acad. Sci. U.S.A.* **108**, 4129–4134 [CrossRef Medline](#)
54. Jin, F., Jiang, K., Ji, S., Wang, L., Ni, Z., Huang, F., Li, C., Chen, R., Zhang, H., Hu, Z., and Zha, X. (2017) Deficient TSC1/TSC2-complex suppression of SOX9-osteopontin-AKT signalling cascade constrains tumour growth in tuberous sclerosis complex. *Hum. Mol. Genet.* **26**, 407–419 [Medline](#)